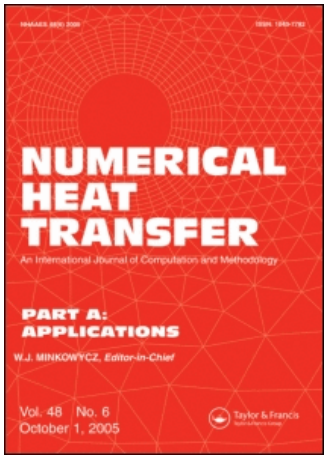

Numerical Heat Transfer, Part A: Applications
An International Journal of Computation and Methodology
Publication details, including instructions for authors and subscription information:
http://www.informaworld.com/smpp/title~content=t713657973

HEAT TRANSFER IN FEMTOSECOND LASER PROCESSING OF METAL

Ihtesham H. Chowdhury [a]; Xianfan Xu [a]
[a] School of Mechanical Engineering, Purdue University, West Lafayette, Indiana, USA.

Online Publication Date: 01 August 2003
To cite this Article: Chowdhury, Ihtesham H. and Xu, Xianfan (2003) 'HEAT TRANSFER IN FEMTOSECOND LASER PROCESSING OF METAL', Numerical Heat Transfer, Part A: Applications, 44:3, 219 - 232
To link to this article: DOI: 10.1080/716100504
URL: http://dx.doi.org/10.1080/716100504

Numerical Heat Transfer, Part A, 44: 219–232, 2003

ISSN: 1040-7782 print/1521-0634 online
DOI: 10.1080/10407780390210224

Taylor & Francis
Taylor & Francis Group

HEAT TRANSFER IN FEMTOSECOND LASER PROCESSING OF METAL

Ihtesham H. Chowdhury and Xianfan Xu
School of Mechanical Engineering, Purdue University, West Lafayette, Indiana, USA

The short time scales and high intensities obtained during femtosecond laser irradiation of metals require that heat transfer calculations take into account the nonequilibrium that exists between electrons and the lattice during the initial laser heating period. Thus, two temperature fields are necessary to describe the process—the electron temperature and the lattice temperature. In this work, a simplified one-dimensional, parabolic, two-step model is solved numerically to predict heating, melting, and evaporation of metal under femtosecond laser irradiation. Kinetic relations at the phase-change interfaces are included in the model. The numerical results show close agreement with experimental melting threshold fluence data. Further, it is predicted that the solid phase has a large amount of superheating and that a distinct melt phase develops with duration of the order of nanoseconds.

INTRODUCTION

In the last few years, the use of femtosecond lasers in materials processing and related heat transfer issues has been studied both theoretically and experimentally. Several reviews of the topic can be found in the literature [1]. This interest has been sparked by the fact that ultrashort lasers offer considerable advantages in machining applications, chief among which are the abilities to machine a wide variety of materials and to machine extremely small features with minimal debris formation.

In general, three different heat transfer regimes during femtosecond laser irradiation of metals have been identified [2]. These are illustrated in Figure 1. Initially, the free electrons absorb the energy from the laser and this stage is characterized by a lack of thermal equilibrium among the electrons. In the second stage, the electrons reach thermal equilibrium and the density of states can now be represented by the Fermi distribution. However, the electrons and the lattice are still at two different temperatures, and heat transfer is mainly due to diffusion of the hot electrons. In the final stage, the electrons and the lattice reach thermal equilibrium and normal thermal diffusion carries the energy into the bulk. A two-temperature model to predict the

Received 21 May 2002; accepted 28 November 2002.

Support for this work by the U.S. Office of Naval Research is greatly appreciated. I. H. Chowdhury also acknowledges support by Purdue University in the form of a Presidential Distinguished Graduate Fellowship.

Address correspondence to X. Xu, School of Mechanical Engineering, Purdue University, West Lafayette, IN 47907-1288, USA. E-mail: xxu@ecn.purdue.edu

NOMENCLATURE

A	coefficient in Eq. (14)
B_e	coefficient in Eq. (7)
C	heat capacity
d	thickness of the sample
G	electron–lattice coupling factor
H	enthalpy
J	laser pulse fluence
j_v	molar evaporation flux
k_b	Boltzmann's constant
L_{lv}	latent heat of evaporation
L_{sl}	latent heat of melting
M	molar weight
$\mathbf{Q}$	heat flux
Q_a	heat source term
R	surface reflectivity
R_u	universal gas constant
S	laser source term
t	time
t_p	laser pulse width, full width at half maximum (FWHM)
T	temperature
T_b	equilibrium boiling temperature
T_c	critical temperature
T_F	Fermi temperature
T_m	equilibrium melting temperature
V	velocity
V_o	velocity factor in Eq. (11)
x	spatial coordinate
α	thermal diffusivity
δ	radiation penetration depth
δ_b	ballistic depth
ΔT	interface superheating
ε_F	Fermi energy of gold
η	coefficient in Eq. (8)
ϑ	coefficient in Eq. (8)
κ	thermal conductivity
ρ	density
τ	electron relaxation time
χ	coefficient in Eq. (8)

Subscripts

0	reference temperature
e	electron
l	lattice
liq	liquid
lv	liquid–vapor interface
s	solid
sl	solid–liquid interface

nonequilibrium temperature distribution between electrons and the lattice during the second regime was first described by Anisimov et al. [3]. Subsequently, Qiu and Tien [4] rigorously derived a hyperbolic two-step model from the Boltzmann transport equation. This model looks at the heating mechanism as consisting of three processes: the absorption of laser energy by the electrons, the transport of energy by the electrons, and heating of the lattice by electron–lattice interactions. Qiu and Tien [5] calculated application regimes for the one-step and two-step heating processes and also regimes for hyperbolic and parabolic heating. They concluded that for fast heating at higher temperature, the laser pulse duration is much longer than the electron relaxation time. As such, the hyperbolic two-step (HTS) model, which accounts for the electron relaxation time, can be simplified to the parabolic two-step (PTS) model. The HTS and PTS models have been solved numerically for femtosecond laser heating of various metals at relatively low fluences and the results have been shown to agree well with experiments. Approximate analytical solutions for the two-step equations have been developed by Anisimov and Rethfeld [6] and by Smith et al. [7]. Chen and Beraun [8] reported a numerical solution of the HTS model using a mesh-free particle method. An alternative approach to the problem has been developed by Tzou and Chiu [9]. They developed a dual-phase-lag (DPL) model wherein the two-step energy transport is regarded as a lagging behavior of the energy carriers. Their model predictions show reasonably close agreement with experimentally observed temperature changes in gold thin-film samples.

Most of the numerical solutions of the two-step model reported in the literature have concentrated on temperatures well below the phase-change temperature.

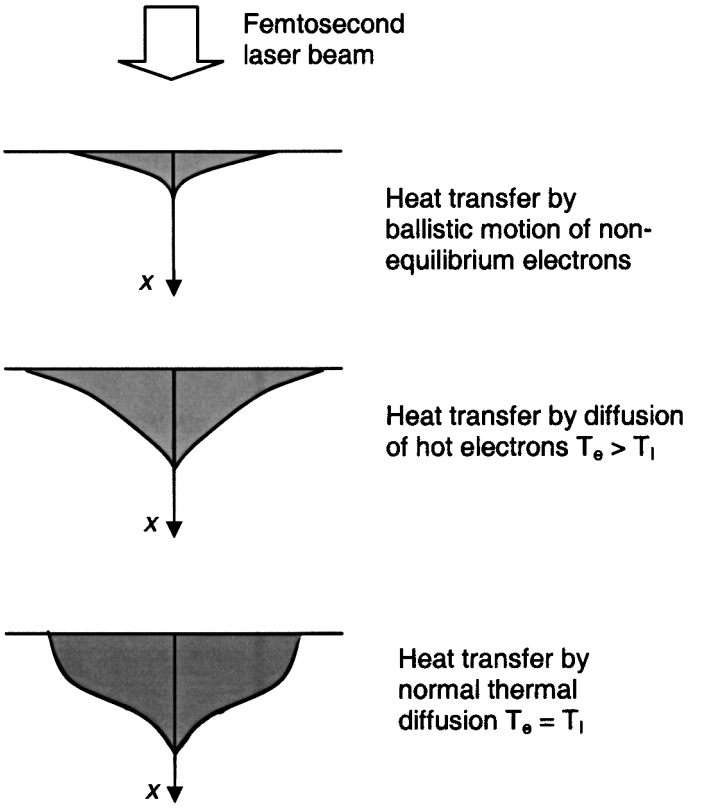

Figure 1. Three stages of energy transfer during femtosecond laser irradiation (adapted from [2]).

Kuo and Qiu [10] extended the PTS model to simulate the melting of metal films exposed to picosecond laser pulses. The present work extends the numerical solution of the one-dimensional PTS model to include both melting and evaporation effects on irradiation of metal with much shorter pulses, of femtosecond duration. Heating above the normal melting and boiling temperatures is allowed by including the appropriate kinetic relations in the computation. Therefore, the main difference between this work and prior work is that evaporation process and its effect on energy transfer and material removal is studied. It is seen that with increasing pulse energy, there is considerable superheating and the solid–liquid interface temperature approaches the boiling temperature. However, the surface evaporation process does *not* contribute significantly to the material-removal process.

NUMERICAL MODELING

In general, the conduction of heat during a femtosecond pulsed laser heating process is described by a nonequilibrium hyperbolic two-step model [4]. The equation for this model are given below:

$$C_e(T_e)\frac{\partial T_e}{\partial t} = -\nabla \cdot \mathbf{Q} - G(T_e - T_l) + S \tag{1}$$

$$C_l \frac{\partial T_l}{\partial t} = \nabla[\kappa_l(\nabla T_l)] + G(T_e - T_l) \tag{2}$$

$$\tau \frac{\partial \mathbf{Q}}{\partial t} + \kappa_e T_e + \vec{Q} = 0 \tag{3}$$

The first equation describes the absorption of heat by the electron system from the laser, the heat diffusion among the electrons, and transfer of heat to the lattice. S is the laser heating source term, defined later. The second equation is for the lattice and contains a heat diffusion term and the energy input term due to coupling with the electron system. The third equation provides for the hyperbolic effect. If Eqs. (1) and (3) are combined, a dissipative wave equation characteristic of hyperbolic heat conduction is obtained. Tang and Araki [11] have shown that the solution of the dissipative wave equation yields a temperature profile with distinct wavelike characteristics. In Eq. (3), τ is the electron relaxation time, which is the mean time between electron–electron collisions. Qiu and Tien [5] have calculated the value of τ to be of the order of 10 fs for gold. In this study, the pulse widths are of the order of 100 fs, which is much longer than τ, and the temperatures are also much above room temperature so that τ is further reduced. As such, the hyperbolic effect can be neglected and the HTS equations can be simplified to a parabolic two-step (PTS) model. The equations can be further simplified to consider only one-dimensional heat conduction, as the laser beam diameter is much larger than the heat penetration depth. The one-dimensional forms of the equations of the PTS model used in the simulation are

$$C_e(T_e) \frac{\partial T_e}{\partial t} = \frac{\partial}{\partial x}\left(\kappa_e \frac{\partial T_e}{\partial x}\right) - G(T_e - T_l) + S \tag{4}$$

$$C_l \frac{\partial T_l}{\partial t} = \frac{\partial}{\partial x}\left(\kappa_l \frac{\partial T_l}{\partial x}\right) + G(T_e - T_l) \tag{5}$$

The laser heating source term S is given as [2, 5]

$$S = 0.94 \frac{1 - R}{t_p(\delta + \delta_b)(1 - e^{-d/(\delta+\delta_b)})} J \cdot \exp\left[-\frac{x}{(\delta + \delta_b)} - 2.77\left(\frac{t}{t_p}\right)^2\right] \tag{6}$$

A temporal Gaussian pulse has been assumed where time $t = 0$ is taken to coincide with the peak of the pulse. Equation (6) describes the absorption of laser energy in the axial direction where the depth parameter $x = 0$ at the free surface. t_p is the FWHM (full width at half maximum) pulse width, δ the absorption depth, R the reflectivity, d the thickness of the sample, and J the fluence. δ_b is the ballistic range, which provides for the ballistic transport of energy by the hot electrons. The ballistic transport of electrons was shown in a pump-probe reflectivity experiment on thin gold films [2]. Homogeneous heating was observed in thin films of thickness less than 100 nm. At thicknesses greater than this, diffusive motion dominates and cause the change from linear to exponential decay. It has been reported that using the ballistic parameter leads to better agreement between predictions and experimental data on heating by a femtosecond laser pulse [2, 8].

The electronic heat capacity is taken to be proportional to the electron temperature with a coefficient B_e [5]:

$$C_e(T_e) = B_e T_e \tag{7}$$

The electron thermal conductivity is generally taken to be proportional to the ratio of the electron temperature and the lattice temperature [5]. This is valid for the case where the electon temperature is much smaller than the Fermi temperature $T_F(= \varepsilon_F/k_b)$. For gold, which is the material investigated in the simulations, the Fermi temperature is 6.42×10^4 K. However, for the high energy levels considered here, the electron temperatures becomes comparable to the Fermi temperature and a more general expression valid over a wider range of temperatures has to be used [6]:

$$\kappa_e = \chi \frac{(\vartheta_e^2 + 0.16)^{1.25}(\vartheta_e^2 + 0.44)\vartheta_e}{\sqrt{\vartheta_e^2 + 0.092}(\vartheta_e^2 + \eta\vartheta_1)} \tag{8}$$

where $\vartheta_e = k_b T_e/\varepsilon_F$ and $\vartheta_l = k_b T_l/\varepsilon_F$.

The simulation is started at time $t = -2t_p$. The initial electron and lattice temperatures are taken to be equal to the room temperature and the top and bottom surfaces of the target are assumed to be insulated, leading to the initial and boundary conditions:

$$T_e(x, -2t_p) = T_l(x, -2t_p) = T_0 \tag{9}$$

$$\left.\frac{\partial T_e}{\partial x}\right|_{x=0} = \left.\frac{\partial T_e}{\partial x}\right|_{x=d} = \left.\frac{\partial T_1}{\partial x}\right|_{x=0} = \left.\frac{\partial T_1}{\partial x}\right|_{x=d} = 0 \tag{10}$$

At the high fluences and short pulse widths considered in this study, rapid phase changes are controlled by nucleation dynamics rather than by heat transfer at the solid–liquid or liquid–vapor interface. At the solid–liquid interface, the relation between the superheating/undercooling at the interface, $\Delta T = T_{sl} - T_m$, and the interface velocity V_{sl} is given by [12]

$$V_{sl}(T_{sl}) = V_0\left[1 - \exp\left(-\frac{L_{sl}\Delta T}{k_b T_{sl} T_m}\right)\right] \tag{11}$$

where T_{sl} is the temperature of the solid–liquid interface, T_m the equilibrium melting temperature, and L_{sl} is the enthalpy of fusion per atom. V_0 is a velocity factor. The energy balance equation at the solid–liquid interface is

$$\kappa_s \left.\frac{\partial T_l}{\partial x}\right|_s - \kappa_{\text{liq}} \left.\frac{\partial T_1}{\partial x}\right|_{\text{liq}} = \rho_s V_{sl} L_{sl} \tag{12}$$

At the liquid–vapor interface, if it is assumed that the two phases are in mechanical and thermal equilibrium, that the specific volume of the vapor is much larger that of the liquid, and that the ideal gas law applies, then the

Clausius-Clapeyron equation can be applied to calculate the saturation pressure at the surface temperature. Considering also the change in latent heat of vaporization L_{lv} with the liquid–vapor interfacial temperature T_{lv}, a relation between the saturation pressure p and T_{lv} can be found as [12]

$$p = p_0 \exp\left\{ -\frac{L_0}{R_u}\left[\frac{1}{T_{lv}}\sqrt{1-\left(\frac{T_{lv}}{T_c}\right)^2} - \frac{1}{T_b}\sqrt{1-\left(\frac{T_b}{T_c}\right)^2}\right]. \right.$$
$$\left. -\frac{L_0}{R_u T_c}\left[\sin^{-1}\left(\frac{T_{lv}}{T_c}\right) - \sin^{-1}\left(\frac{T_b}{T_c}\right)\right]\right\} \tag{13}$$

where L_0 is the latent heat of vaporization at absolute zero, R_u the universal gas constant, T_b the equilibrium boiling temperature, and T_c the critical temperature.

The liquid–vapor interfacial velocity can then be obtained from the molar flux j_v as [12]

$$V_{lv} = \frac{Mj_v}{\rho_{\text{liq}}} = \frac{AMp}{\rho_{\text{liq}}\sqrt{2\pi M R_u T_{lv}}} \tag{14}$$

where M is the molecular weight. A is a coefficient that accounts for the backflow of evaporated vapor to the surface and has been calculated to be 0.82 [12]. The energy balance equation at the liquid–vapor interface is

$$\kappa_{\text{liq}} \frac{\partial T_1}{\partial x}\bigg|_{\text{liq}} = \rho_{\text{liq}} V_{lv} L_{lv} \tag{15}$$

The above expressions for surface evaporation assume small deviation from equilibrium. In pulsed laser heating, the kinetic equation at the liquid–vapor interface could deviate significantly from the Clausius–Clapeyron equation [13]. However, it will be shown later that the accuracy of the interface relation does not affect the numerical results, since the energy carried away by evaporation accounts for a very small fraction of the total energy transfer, and the amount of the material removed by evaporation is insignificant.

The governing equations (4) and (5) are solved using the finite-difference method. The domain is divided into fixed grids in the axial direction x. Two values, electron temperature and lattice temperature, are then assigned to each node. To solve for the lattice temperature field and the related phase changes, the enthalpy formulation is used. Equation (4) is cast in terms of enthalpy per unit volume as

$$\frac{\partial H}{\partial t} = \frac{\partial}{\partial x}\left(\kappa_t \frac{\partial T_t}{\partial x}\right) + Q_a(x,t) \tag{16}$$

where H is the sum of the sensible enthalpy and latent heat. The interface energy balances are embedded in the enthalpy equation, thus the melt and vapor interfaces are tracked implicitly.

An averaged enthalpy within a control volume can be calculated as the sum of sensible enthalpy and latent heat as

$$H = \int_{T_0}^{T} \rho c_e dT + f_{\text{liq}} \rho_{\text{liq}} L_{sl} + f_v \rho_{\text{liq}} L_{lv} \tag{17}$$

This completes the equations needed for the numerical model. The procedure followed for the solution of these equations is outlined below.

1. Both the electron and lattice temperature fields are set to the ambient temperature, and the melting and boiling temperatures are set to the equilibrium melting and boiling temperatures.
2. The electron temperature field is calculated by the semi-implicit Crank-Nicholson method.
3. The resulting electron temperatures are used to calculate the amount of energy that will be transferred to the lattice, and the lattice temperature field is computed as described in the following steps.
4. Below the melting point, the calculation of temperature is straightforward. Once the melting point is reached, an interfacial temperature, T_{sl}, is assumed and the fraction of liquid, f_{liq}, in each cell is calculated. This is done using the explicit method.
5. The position of the solid–liquid interface is then obtained from the values of the liquid fractions. This gives an estimate of the velocity V_{sl} and Eq. (11) can then be used to get a new estimate for T_{sl}.
6. Steps 4 and 5 are repeated until the velocity V_{sl} converges according to the following criterion: $\max \left| \left(V_{sl}^{\text{new}} - V_{sl}^{\text{old}} \right) \right| \leq 10^{-3}$.
7. When the temperature reaches the boiling point, a calculation similar to steps 5 and 6 is carried out to estimate the liquid–vapor interface temperature using the kinetic relation (13).
8. Steps 3, 4, 5, 6, and 7 are repeated until both the electron and lattice temperature fields converge ($\Delta T_e / T_0 < 10^{-4}$ and $\Delta T_l / T_0 10^{-5}$).
9. The calculation then starts again from step 2 for the next time step.

RESULTS AND DISCUSSION

All the simulations were done for gold, and the thermophysical properties used in the simulation are given in Table 1. No values are available for the electron–lattice coupling factor for liquid gold, so a value which is 20% higher than that of solid gold is assumed [10]. This is thought to be reasonable because atoms in the liquid state lack long-range order and hence electrons collide more frequently with atoms in the liquid state than in the solid state. In a well-conducting metal such as gold, the lattice component of the thermal conductivity comprises only about 1% of the total, the rest being due to the electrons [14]. In order to avoid calculating the electron conductivity twice, the lattice conductivity used in the calculation, κ_l, was taken to be 1% of the value of the bulk conductivity given in Table 1. No experimental data are available for the physical quantities in the superheated and the undercooled state,

Table 1. Thermophysical properties of gold used in the calculation

Coefficient for electronic heat capacity B_e (J/m^3K^2)	70.0 [4]
Specific heat of the solid phase C_s (J/kg K)	$109.579 + 0.128T - 3.4 \times 10^{-4}T^2 + 5.24 \times 10^{-7}T^3 - 3.93 \times 10^{-10}T^4 + 1.17 \times 10^{-13}T^5$ [22]
Specific heat of the liquid phase C_{liq} (J/kg K)	157.194 [22]
Electron–lattice coupling factor G (W/m^3 K) (s, solid liq, liquid)	s, 2.0×10^{16}[2] liq, 2.4×10^{16}
Enthalpy of evaporation L_{lv} at T_b (J/kg)	1.698×10^6 [22]
Enthalpy of fusion L_{sl} (J/kg)	6.373×10^4 [22]
Molar weight M (kg/kmol)	196.967 [22]
Reflection coefficient R	0.36262 [23]
Universal gas constant R_u (J/K mol)	8.314
Boiling Temperature T_b (K)	3,127 [22]
Critical temperature T_c (K)	5,590 [24]
Melting temperature T_m (K)	1,337.58 [22]
Velocity factor V_0 (m/s)	1,300 [10]
Coefficient for electronic conductivity χ (W/mK)	353 [6]
Radiation penetration depth δ (nm)	18.22 [23]
Fermi energy ε_F (eV)	5.53 [23]
Thermal conductivity of the solid phase κ_s (W/mK)	$320.973 - 0.0111T - 2.747 \times 10^{-5}T^2 - 4.048 \times 10^{-9}T^3$ [25]
Thermal conductivity of the liquid phase κ_{liq} (W/mK)	$37.72 + 0.0711T - 1.721 \times 10^{-5}T^2 + 1.064 \times 10^{-9}T^3$ [25]
Solid density ρ_s (kg/m^3)	19.3×10^3
Liquid density ρ_{liq}(kg/m^3)	17.28×10^3

so the values of the material properties at the melting point are used for these nonequilibrium states.

In most of the calculations, a total of 300 grid points was used. Out of these, 150 were put in the top quarter of the domain in a graded fashion so that the grid is finer at the top. The remaining points were placed in a uniform manner in the lower three-quarters of the domain. A time step of 10^{-16} s was used initially. After the electrons and the lattice reached the same temperature, the time step was increased to 10 fs to speed up the calculation. The total input energy and the total energy gained by the system (electrons and lattice) were also tracked. It was found that the difference was less than 0.01% in all cases. A time-step and grid-sensitivity test was also done and it was found that sufficient independence from these parameters was obtained during the calculation.

Figure 2 shows a comparison between the melting threshold fluences predicted by the simulation and the experimental data of Wellershoff et al. [15]. The fluences plotted in the figure are the absorbed fluences $(1 - R)J$. Two sets of results are plotted in the figure—one in which the ballistic depth, δ_b is taken to be 200 nm and the other in which the ballistic effect is neglected completely. It is seen that if the ballistic effect is not considered, the predicted melting threshold fluence is much lower than the experimentally determined value. This is because, in the latter case, the incident laser energy is absorbed only in the absorption depth δ and hence leads to a higher energy density in the top part of the film, which translates into higher temperatures. On the other hand, consideration of the ballistic depth leads to the incident energy being absorbed over a greater depth, which gives a lower

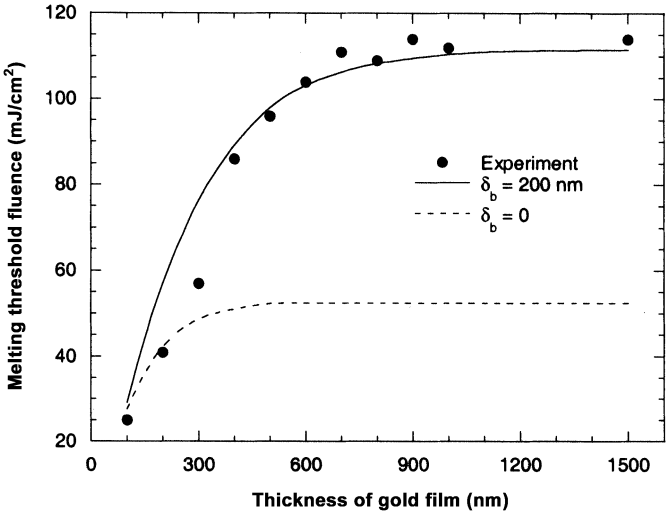

Figure 2. Melting threshold fluence as a function of sample thickness for 200-fs pulses.

temperature and hence higher threshold fluence. The ballistic depth of 200 nm that is considered here is reasonably consistent with previous measurements of the depth, which gave a value of 105 nm for much lower fluence pulses [2].

The inclusion of the ballistic effect gives a reasonably good fit to the experimental data. It is seen that the threshold fluence saturates at about $111\,\mathrm{mJ/cm^2}$ for film thickness greater than 900 nm, which is due to the fact that the sample is thick compared with the electronic diffusion range. Also, it is noticed that the simulation overestimates the fluence for thinner films. This may be due to the fact that multiple reflections that might occur for thinner films are not included in the model. The thermal conductivity of thin metal films has also been shown to be smaller then the bulk value [16]. Taking this effect into account would lower the predicted damage threshold for the thinner films. Also, it has been shown that the value of the electron–lattice coupling factor might change depending on the electron temperature [17]. This has not been considered in the simulation and might improve model accuracy. Smith and Norris [18] have shown that their numerical solution of the PTS model predicts higher lattice temperatures when the temperature dependence of the electron–phonon coupling factor is taken into account.

The second stage of the calculation included phase-change phenomena. In all of these calculations, a ballistic depth $\delta_b = 200\,\mathrm{nm}$ was assumed in accordance with the threshold calculations discussed above. In order to simplify the calculation, the relation between the liquid–vapor interface velocity V_{lv} and the liquid–vapor interface temperature T_{lv} was calculated according to Eq. (14). A curve was fitted to the calculated values and is plotted in Figure 3. It is noticed that the maximum velocity at which the liquid–vapor interface can move is limited by the value of the critical temperature T_c which is 5,590 K. At the critical temperature, the interface velocity is about 0.3 m/s. In general, $0.9T_c$ is the maximum temperature to which a liquid can be superheated, at which a volumetric phase-change phenomenon, called phase explosion, would occur [19]. However, the current model is not able to compute

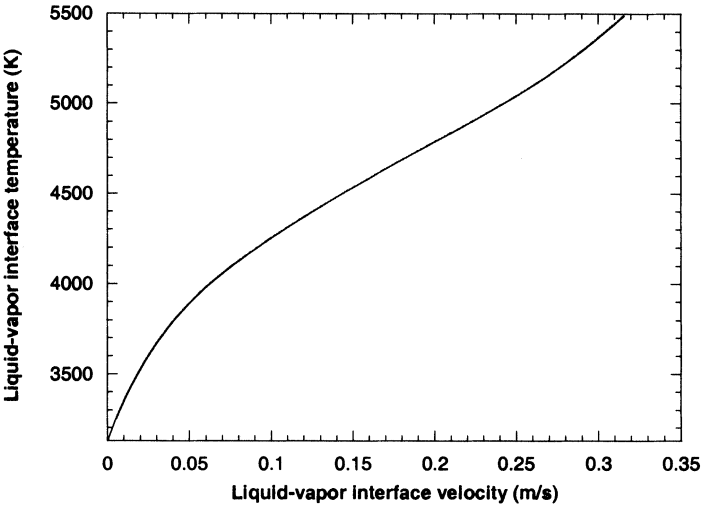

Figure 3. Plot of liquid–vapor interface temperature as a function of interface velocity.

phase explosion. As the time scales of interest are very small—of the order of 1 ns—the maximum amount of vaporization that is predicted by Eq. (14) is very small (~ 0.1 nm), even smaller than the lattice constant of gold (0.407 nm). This implies that a mechanism such as phase explosion is responsible for the material removal process at higher laser fluences.

Because of the small amount of evaporation, in all the calculations where the temperature of the liquid exceeded the normal boiling temperature of 3,127 K, the material removal by evaporation was neglected and the thermal effect due to vaporization was treated as a surface heat transfer boundary condition at $x = 0$ as given in Eq. (15). It was also found from the calculation that changing the value of V_{lv} did not make any appreciable difference to the results, owing to the fact that the heat removal by evaporation is small compared with the heat input from the laser. In order to speed up the calculation, the value of V_{lv} was kept constant at 0.3 m/s in the calculations shown below.

Four sets of results are presented in Figures 4–7 for four different fluence levels ranging from just above the melt threshold at 0.2 J/cm^2 to 0.5 J/cm^2, where the surface temperature just exceeds $0.9T_c$. In all these cases, the pulse width was kept constant at 100 fs FWHM and the total size of the calculation domain was 10 μm. Figure 4 shows the variation of the lattice temperature at the surface ($x = 0$) with time. It was found that the peak temperature was reached at times of 40.9, 58.0, 64.6, and 71.2 ps, respectively, at absorbed laser fluences of 0.2, 0.3, 0.4, and 0.5 J/cm^2. All these are times much after the end of the laser pulse. The time lag between the energy input and the response of the lattice is due to the two-temperature effect in which the energy is absorbed by the electrons first and then coupled to the lattice slowly. It was seen from the calculation that it took approximately 48, 58, 65, and 71 ps for the lattice and the electrons to reach thermal equilibrium in the four cases. It is noticed that this time increases as the fluence is increased, which is to be expected as a higher fluence leads to a large initial nonequilibrium. Also, it is seen that at a fluence level of

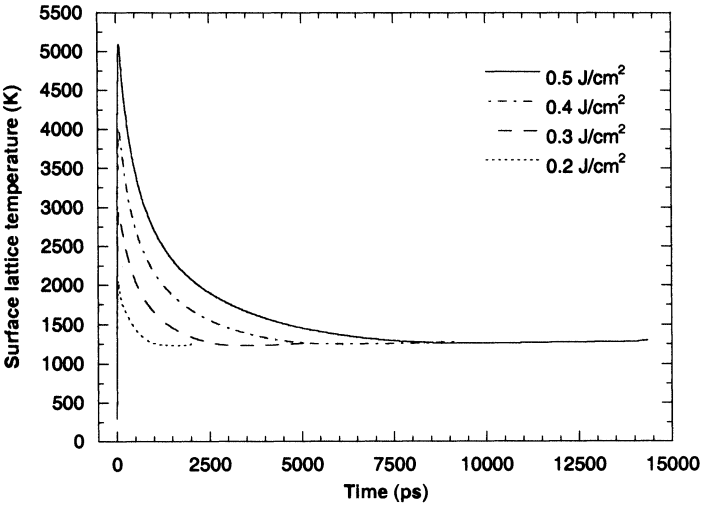

Figure 4. Plot of surface lattice temperature as a function of time for a 100-fs FWHM pulse at four different fluence levels.

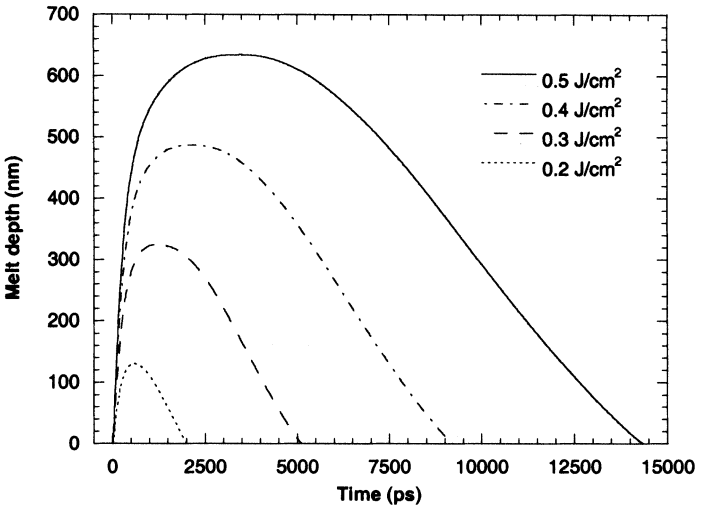

Figure 5. Plot of melt depth as a function of time for a 100-fs FWHM pulse at four different fluence levels.

$0.5\,J/cm^2$, the peak temperature slightly exceeds $0.9T_c$ (5,031 K). Thus, fluence levels higher than this would definitely drive the material into the phase explosion regime, which is not provided for in the current model.

Figure 5 shows the melt depths that are predicted by the calculation. It is noticed that, like the temperature, the melting is also delayed and occurs much after the end of the pulse. The melt depth gradually increases with increasing fluence and reaches several hundreds of nanometers, and the melt duration is of the order of nanoseconds. It was seen that melting began at 11.7, 8.7, 7.2, and 6.3 ps, respectively, for the fluence levels of 0.2, 0.3, 0.4, and $0.5\,J/cm^2$ considered in the simulation.

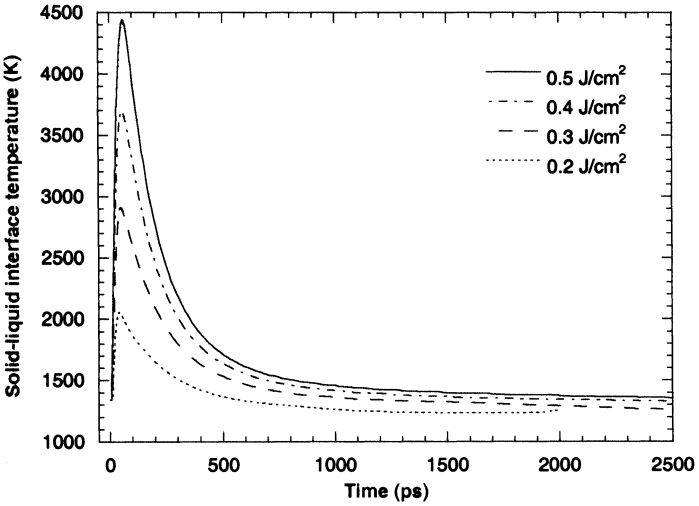

Figure 6. Plot of solid–liquid interface temperature as a function of time for a 100-fs FWHM pulse at four different fluence levels.

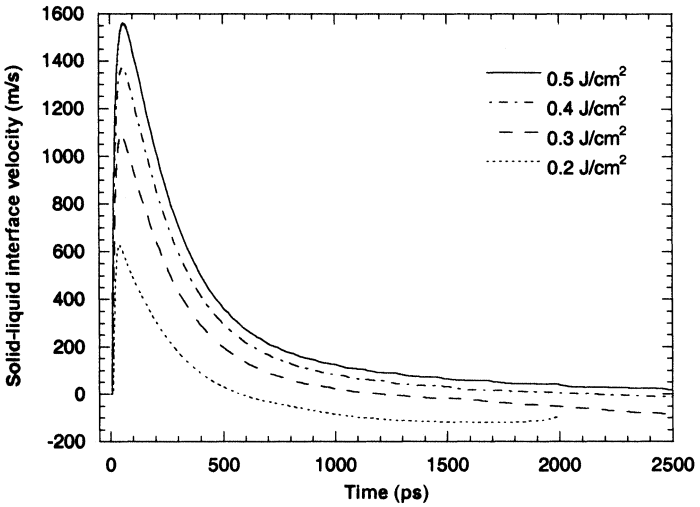

Figure 7. Plot of solid–liquid interface velocity as a function of time for a 100-fs FWHM pulse at four different fluence levels.

Similar delays in the beginning of melting were observed during experiments on aluminum films irradiated by 20-ps pulses [20]. The phase change was detected by the scattering of electrons transmitted through the sample and subsequent recording of the diffraction pattern. It was noticed that the onset of melting was delayed and that the delay decreased with increasing fluence as seen in the present simulation.

Figures 6 and 7 show the evolution of the solid–liquid interface temperature and velocity, respectively. It is noted that the values of superheating are very high. In two cases, it is seen that the solid–liquid interface temperature even exceeds the

normal boiling temperature T_b. This is also reflected in the prediction of the interface velocity, which is of the order of 1,000 m/s—much higher than those usually reported for slower nanosecond laser heating processes. Some experimental results seem to support these predictions [21]. In that work, the melting interfacial velocities in gold samples of 50- and 100-nm thicknesses irradiated with 40-ps laser pulses were found to be as high as 1,400 m/s.

CONCLUSIONS

A general numerical solution of the PTS model for heating, melting, and evaporation of metal has been developed. The melting threshold fluences predicted by the simulation agree well with experimental data reported in the literature. The simulation results indicate that the phase-change phenomena during femtosecond heating of metal are highly nonequilibrium, consistent with the extremly short time scales involved. A considerable amount of superheating of the solid phase was observed, and consequently, very high melting interfacial velocities were predicted. It was also seen that normal evaporation cannot account for the material removal and that the lattice temperatures could rise to as much as $0.9T_c$ at fairly modest fluences. This implies that a mechanism such as phase explosion might be responsible for the material removal process at higher laser fluences.

REFERENCES

1. M. D. Shirk and P. A. Molian, A Review of Ultrashort Pulsed Laser Ablation of Materials, *J. Laser Appl.*, vol. 10, pp. 18–28, 1998.
2. J. Hohlfeld, S.-S. Wellershoff, J. Güdde U. Conrad, V. Jähnke, and E. Matthias, Electron and Lattice Dynamics following Optical Excitation of Metals, *Chem. Phys.*, vol. 251, pp. 237–258, 2000.
3. S. I. Anisimov, B. L. Kapeliovich, and T. L. Perel'man, Electron Emission from Metal Surfaces Exposed to Ultrashort Laser Pulses, *Sov. Phys. JETP*, vol. 39, pp. 375–377, 1974.
4. T. Q. Qiu and C. L. Tien, Heat Transfer Mechanisms during Short-Pulse Laser Heating of Metals, *ASME J. Heat Transfer*, vol. 115, pp. 835–841, 1993.
5. T. Q. Qiu and C. L. Tien, Femtosecond Laser Heating of Multi-Layer Metals—I. Analysis, *Int. J. Heat Mass Transfer*, vol. 37, pp. 2789–2797, 1994.
6. S. I. Anisimov and B. Rethfeld, On the Theory of Ultrashort Laser Pulse Interaction with a Metal, *Proc. Nonresonant Laser-Matter Interaction* (NLMI-9), vol. 3093, St. Petersburg, Russia, pp. 192–203, SPIE, Bellingham, Washington, DC, 1997.
7. A. N. Smith, J. L. Hostetler, and P. M. Norris, Nonequilibrium Heating in Metal Films: An Analytical and Numerical Analysis, *Numer. Heat Transfer A*, vol. 35, pp. 859–873, 1999.
8. J. K. Chen and J. E. Beraun, Numerical Study of Ultrashort Laser Pulse Interactions with Metal Films, *Numer. Heat Transfer A*, vol. 40, pp. 1–20, 2001.
9. D. Y. Tzou and K. S. Chiu, Temperature-Dependent Thermal Lagging in Ultrafast Laser Heating, *Int. J. Heat Mass Transfer*, vol. 44, pp. 1725–1734, 2001.
10. L.-S. Kuo and T. Q. Qiu, Microscale Energy Transfer during Picosecond Laser Melting of Metal Films, *Proc. 31st Natl. Heat Transfer Conf.*, Houston, TX, pp. 149–157, ASME, New York, 1996.
11. D. W. Tang and N. Araki, The Wave Characteristics of Thermal Conduction in Metallic Films Irradiated by Ultra-Short Laser Pulses, *J. Phys. D—Appl. Phys.*, vol. 29, pp. 2527–2533, 1996.

12. X. Xu, G. Chen, and K. H. Song, Experimental and Numerical Investigation of Heat Transfer and Phase Change Phenomena during Excimer Laser Interaction with Nickel, *Int. J. Heat Mass Transfer*, vol. 42, pp. 1371–1382, 1999.
13. X. Xu and D. A. Willis, Non-equilibrium Phase Change in Metal Induced by Nanosecond Pulsed Laser Irradiation, *J. Heat Transfer*, vol. 124, pp. 293–298, 2002.
14. P. G. Klemens and R. K. Williams, Thermal Conductivity of Metals and Alloys, *Int. Metals Rev.*, vol. 31, pp. 197–215, 1986.
15. S.-S. Wellershoff, J. Hohlfeld, J. Güdde, and E. Matthias, The Role of Electron-Phonon Coupling in Femtosecond Laser Damage of Metals, *Appl. Phys. A*, vol. 69, pp. S99–S107, 1999.
16. C. A. Paddock and G. L. Eesley, Transient Thermoreflectance from Thin Metal Films, *J. Appl. Phys.*, vol. 60, pp. 285–290, 1986.
17. W. S. Fann, R. Storz, H. W. K. Tom, and J. Bokor, Direct Measurement of Non-equilibrium Electron-Energy Distributions in Subpicosecond Laser-Heated Gold Films, *Phys. Rev. Lett.*, vol. 68, pp. 2834–2837, 1992.
18. A. N. Smith and P. M. Norris, Numerical Solution for the Diffusion of High Intensity, Ultrashort Laser Pulses within Metal Films, *Proc. 11th Int. Heat Transfer Conf.*, Kyongju, Korea, vol. 5, pp. 241–246, Taylor & Francis, London, UK, 1998.
19. K. H. Song and X. Xu, Explosive Phase Transformation in Pulsed Laser Ablation, *Appl. Surface Sci.*, vol. 127, pp. 111–116, 1998.
20. S. Williamson, G. Mourou, and J. C. M. Li, Time-Resolved Laser-Induced Phase Transformation in Aluminum, *Phys. Rev. Lett.*, vol. 52, pp. 2364-2367, 1984.
21. B. E. Homan, M. T. Connery, D. E. Harrison, and C. A. MacDonald, Measurements of Melting Velocities in Gold Films on a Picosecond Time Scale, *Proc. Symp. Beam-Solid Interactions: Fundamentals and Applications*, Boston, vol. 279, pp. 717–722, Material Research Society, Pittsburgh, PA, 1993.
22. I. Barin, *Thermochemical Data of Pure Substances Part 1*, pp. 92–93, VCH, New York, 1993.
23. B. H. Billings (ed.), *American Institute of Physics Handbook*, McGraw-Hill, New York, 1972.
24. M. M. Martynyuk, Critical Constants of Metals, *Russ. J. Phys. Chem.*, vol. 57, pp. 494–500, 1983.
25. Y. S. Touloukian, R. W. Powell, C. Y. Ho, and P. G. Klemens, *Thermophysical Properties of Matter*, vol. 1, pp. 132–137, IFI/Plenum, New York–Washington, DC, 1970.